PHOTONICS Research

Enhancement of femtosecond laser-induced surface ablation via temporal overlapping double-pulse irradiation

Zhenyuan Lin,[1,2] Lingfei Ji,[2,3] and Minghui Hong[1,*]

[1]Department of Electrical and Computer Engineering, National University of Singapore, Singapore 117576, Singapore
[2]Institute of Laser Engineering, Beijing University of Technology, Beijing 100124, China
[3]e-mail: ncltji@bjut.edu.cn
*Corresponding author: elehmh@nus.edu.sg

Received 30 September 2019; revised 29 November 2019; accepted 14 December 2019; posted 18 December 2019 (Doc. ID 379254); published 12 February 2020

This paper reports the physical phenomenon of the temporal overlapping double femtosecond laser-induced ablation enhancement at different time delays. Detailed thermodynamic modeling demonstrates the ablation enhancement is highly dependent on the first pulse's laser fluence. In the case of the first pulse laser fluence being higher than material's ablation threshold, the ablation enhancement is attributed to optical absorption modification by the first pulse ablation. While the first pulse's laser fluence is lower than the material's ablation threshold, the first pulse-induced melting leads to much higher absorption of the second pulse. However, for the case of the first pulse's laser fluence even lower than melting threshold, the ablation enhancement decreases obviously with time delay. The results of the temporal overlapping double femtosecond laser ablation of poly(ε-caprolactone) are in good agreement with the theoretical predictions.

https://doi.org/10.1364/PRJ.379254

1. INTRODUCTION

Laser interaction with materials which is determined by material properties and laser processing parameters, is a complex process involving multiple stages [1–3]. Femtosecond laser micromachining has shown its unique advantage to confine the amount of thermal diffusion due to short heating duration and rapid solid-to-vapor phase transition [4–6]. This fast energy deposition enables the femtosecond laser to be a versatile tool in processing materials for a smaller heat-affected zone, better quality ablation crater, and higher ablation rate. However, using a single femtosecond laser pulse can only exert limited impact on the ablation by changing laser processing parameters like pulse energy and pulse duration. To achieve effective ablation, it requires high power or multiple pulses in the femtosecond laser fabrication. Double-pulse femtosecond laser processing is used for surface ablation, and it has been shown to be a useful means to control material removal [7–10]. For different substrate materials, the double-pulse ablation mechanism is different. In the double-pulse femtosecond experiments for metals, when the time delay τ_d between the pulses is equal or longer than the electron-ion relaxation time τ_{ei}, the efficiency of double-pulse-induced ablation decreases with respect to single-pulse irradiation [11–13]. For semiconductors, free-electron density is a crucial parameter for the evaluation of the ablation threshold of materials. In the case of double-pulse laser irradiation, the free electrons in semiconductors, such as Si and TiO_2, can be excited by the first pulse irradiation. These free electrons cannot recombine with holes within 500 fs, which reduces the ablation threshold and allows the second pulse (SP) to generate enhanced ablation [14–16]. Different from metal and semiconductors, the ablation of dielectric materials undergoes nonlinear processes, including avalanche and multiphoton ionization [17–19]. The femtosecond laser irradiation can lead to a fast transient modification within pulse duration. For the double-pulse ablation of dielectric (fused silica), Nagata *et al.* believed that the first pulse (FP) functions as the preconditioning pulse and the SP effectively induces ablation [20]. Most of the reported studies are mainly focused on double-pulse-induced enhancement under the subpulses with laser fluence higher than the ablation threshold [21–23]. However, for the femtosecond laser ablation, the samples' optical properties, such as absorption coefficient, can also be modified under the laser fluence lower than the ablation threshold within dozens of femtoseconds. This fast transient modification can be fully applied for the ablation enhancement by the following pulse duration at a short time delay close to pulse duration. Therefore, the related physical process and mechanism are completely different for us to explore.

In this paper, we systematically investigate the ablation enhancement by double femtosecond laser pulses at different laser fluences of the FP and different time delays. Under the condition of FP laser fluence higher than the ablation threshold, the optical absorption of the irradiated area increases due to the FP-induced ablation. Thus, the absorption of the SP can be enhanced. In the case of the FP laser fluence lower than the ablation threshold, the ablation enhancement is attributed to the light absorption difference between the liquid phase and solid phase at a time delay < 330 fs. By tuning time delay and total laser fluence, the change of light absorption can generate ablation enhancement of poly(ε-caprolactone) (PCL) film with ablation efficiency up to 338% compared to single-pulse irradiation. The laser fluence ratio between the two pulses can also be changed to further modulate the ablation enhancement of double-pulses irradiation. The understanding of the temporal overlapping double-pulse enhancement in the ultrashort laser micromachining process can significantly broaden its applications.

2. MECHANISM PREDICTION AND EXPERIMENT SETUP

It has been claimed that the fundamental interaction processes between ultrashort lasers and dielectrics can be summarized as follows: (1) acceleration of the seed electrons in the laser field via inverse bremsstrahlung absorption (free carrier absorption); (2) generation of secondary electrons by collisional (avalanche) ionization; (3) electron–phonon coupling, i.e., transfer of energy from the electronic system to the lattice; (4) melting, vaporization, plasma formation, and/or ablation [17,18]. Based on this knowledge, the temporal behavior of the free-electron density in the conduction band $n(t)$ can be described by a rate equation [18,24],

$$\frac{\partial n(t)}{\partial t} = aI(t)n(t) + \sigma_k I^k(t). \tag{1}$$

The first term on the right side of Eq. (1) describes avalanche ionization, and the second term means multiphoton ionization. $I(t)$ is the time-dependent laser intensity and a is the avalanche coefficient. σ_k denotes a k-photon absorption cross section, and k is equal to the smallest number of photons needed to overcome the optical bandgap of the material. Equation (1) demonstrates that the bandgap of a dielectric has a major influence on its ablation efficiency, while the bandgap is affected by the material's temperature. In case of temporal double-pulse irradiation, the free-electron density in the conduction band of the FP and SP can be defined as $n_1(t)$ and $n_2(t)$. Thus, the free-electron density of double-pulse ablation is described by the following equation:

$$\frac{\partial n_1(t)}{\partial t} = aI_1(t)n_1(t) + \sigma_{k1} I_1^k(t), \tag{2}$$

$$\frac{\partial n_2(t)}{\partial t} = aI_2(t)[n_1(t) + n_2(t)] + \sigma_{k2} I_2^k(t). \tag{3}$$

Here $I_1(t)$ and σ_{k1} are time-dependent laser intensity and the k-photon absorption cross section of the FP, while $I_2(t)$ and σ_{k2} are related to the SP. In this case, the absorption of the SP is highly dependent on the FP laser fluence. Stuart *et al.* reported that for a 100-fs laser interaction with dielectric material, only the last part of the laser pulse experiences strong absorption or reflection [24]. Thus, if the SP can be introduced in the last part of the FP, the absorption of the SP should be increased considerably. These free-electron density changes can be described by the femtosecond laser-generated temporal distribution of temperature (for a detailed calculation result of free-electron density at single-pulse and double-pulse irradiation, see Appendix A). As shown in Fig. 1, the temperature distribution of the temporal double-pulse irradiation can be considered in three cases, including the FP laser fluence being higher than ablation threshold, lower than ablation threshold, and lower than the melting threshold. Here, T_m and T_v are the melting temperature and vaporization temperature, respectively. While the FP laser fluence is higher than the ablation threshold, the SP irradiates on the material surface at a time delay (within the pulse duration) after the FP ablation. The ablation results in the change of surface roughness, which leads to the increase of absorption of the SP laser energy, as shown in Fig. 1(a). On the other hand, while the laser fluence of a subpulse is slightly lower than surface ablation, the FP can only melt the target. In this case, the material is required to absorb enough latent heat for phase change from liquid to vapor. While the material's absorption coefficient of the liquid phase is typically much higher than that of the solid phase, the energy absorption of the SP enhances after the FP irradiation, as shown in Fig. 1(b). If the phase difference-induced light absorption increase can overcome the latent heat, the double-pulse irradiation can generate considerable enhancement of surface ablation. This phase-change-induced absorption enhancement allows two subpulses, with laser fluence lower than ablation threshold to achieve effective ablation. However, if the laser fluence of the subpulse is too low, there is a weak melting effect induced by the FP irradiation, which is not beneficial for the surface ablation enhancement, as shown in Fig. 1(c). Thus, the

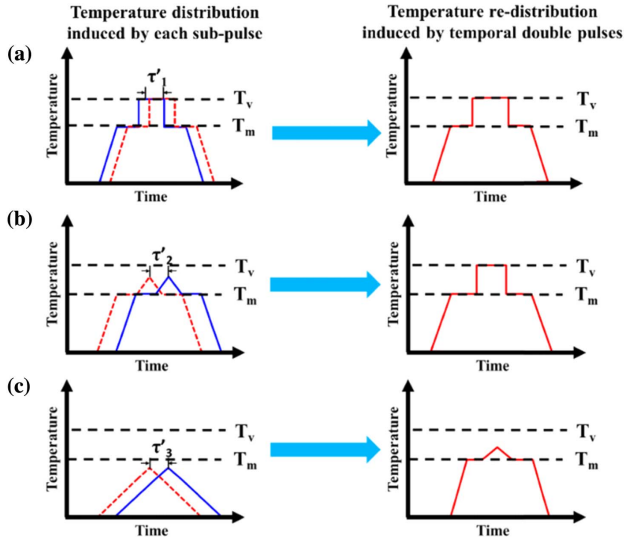

Fig. 1. Schematic diagram of double-pulse laser irradiated temperature field distributions at the FP laser fluence of (a) higher than ablation threshold, (b) lower than ablation threshold, and (c) lower than melting threshold.

temporal femtosecond laser double-pulse-induced ablation should exhibit different behaviors under different laser fluences of the FP.

Based on the above theoretical prediction, the surface ablation experiments are designed and carried out by an 800 nm Ti: sapphire femtosecond laser (Mira 900, Coherent) of 150-fs pulse duration, repetition rate of 80 MHz, and 3 W maximum average power. The double pulses are obtained by a modified Michelson interferometer. As shown in Fig. 2, the laser beam is divided into two parts by a polarizing beam splitter (PBS) and then guided into two arms. One of the two pulses is temporally delayed with respect to the other one by controlling the optical path (arm) length using a precise linear translation stage. In this way, temporal delays $\Delta\tau$ between 0 and 33 ps at a resolution $\Delta\tau$ of ~66 fs are realized between the two parallel polarized pulses. The time delay of temporal double pulses in this study ranges from 0 to 594 fs. A shutter is located in front of a half-wave plate to achieve the desired number of double pulses or single-pulse irradiation. In our experiment, the exposure time is 0.5 s, which means the pulse number is 4×10^7. As the reference for the same total laser power of double-pulse laser ablation, the single-pulse ablation is processed by covering one arm of the interferometer under the case of twice the laser power compared to the double pulse. The half-wave plate allows for tuning laser fluence and different translation stages to adjust the delay individually in each arm. The isolator prevents the laser damage due to strong reflective light from the sample. The two beams are recombined by the other PBS and focused normally onto the target in ambient air by an objective lens of $f = 3.7$ mm with a Gaussian spot of a radius ($1/e^2$) of ~100 μm. The laser ablation is systematically performed on the 20-μm thickness PCL film. Owing to the biocompatibility and biodegradability with good transparency (~90%) of PCL, it has been extensively studied for biological engineering applications such as nanofibers, implants, and drug delivery. The flexible mechanical properties (Young's modulus, elasticity, tensile strength, elongation at break value) of PCL make it suitable for biomedical applications as flexible surface enhanced Raman scattering (SERS) substrates [25,26]. In addition, the surface hydrophilicity of PCL can be modified under excimer laser-induced tissue engineering [27]. The polymer surface is mounted on a computer-controlled x–y–z 3D translation stage and positioned perpendicularly to the beam propagation direction in the focal plane. A laser scanning confocal microscope (LEXT OLS 4100, Olympus) and a surface profiler (Alpha-Step 500, Tencor) are employed to characterize the surface morphology of the ablated samples. In this study, the surface ablation volume is estimated by considering both the depth and diameter of the ablated area depending on the volume formula of the elliptic cylinder: $V = \pi \cdot a \cdot b \cdot h$, or elliptic cone: $V = \pi \cdot a \cdot b \cdot h/3$, where h is the ablation depth, and a and b are semimajor and semiminor axes of ellipse, respectively.

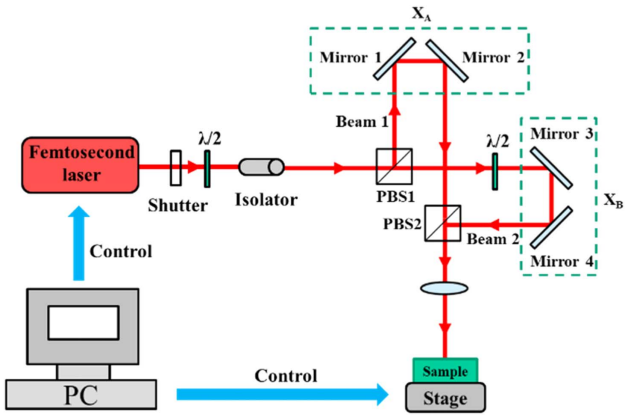

Fig. 2. Schematic diagram of the experimental setup of temporal overlapping double-pulse laser ablation.

3. RESULTS AND DISCUSSION

The laser ablation is systematically performed on the 20-μm thickness PCL films. Prior to the double-pulse experiment, the single-pulse ablation is studied. Figures 3(a)–3(f) show the surface ablation results by the single-pulse femtosecond laser irradiation at a laser fluence of 80−160 μJ/cm^2. The Gaussian distribution of laser irradiation results in ablation and drills holes in the center under 96−160 μJ/cm^2 laser irradiation. Due to the low melting temperature of PCL (about 60°C) and large pulse number, there is an obvious heat-affected zone surrounding the ablation crater. Most of the central craters are the region where the material is completely removed from the PCL film. No surface ablation is observed when the laser fluence is lower than 80 μJ/cm^2. The corresponding horizontal and vertical cross-section profiles of these irradiated samples are shown in Figs. 4(a)–4(d). It can be observed that most of the center hole structures penetrate through the PCL film. In this case, the material removal can also be estimated based on the variation of ablation width. In addition, the anisotropic ablation effect in the horizontal and vertical direction is attributed

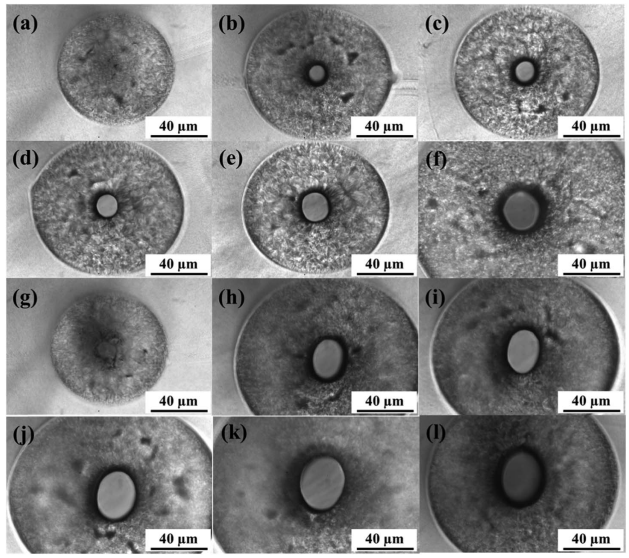

Fig. 3. Surface ablation on PCL film generated by single-pulse femtosecond laser irradiation at different laser fluences. (a) 80, (b) 96, (c) 112, (d) 128, (e) 144, and (f) 160 μJ/cm^2; surface ablation on PCL film generated by double-pulse femtosecond laser irradiation at 264-fs time delay and different total laser fluences: (g) 80, (h) 96, (i) 112, (j) 128, (k) 144, and (l) 160 μJ/cm^2.

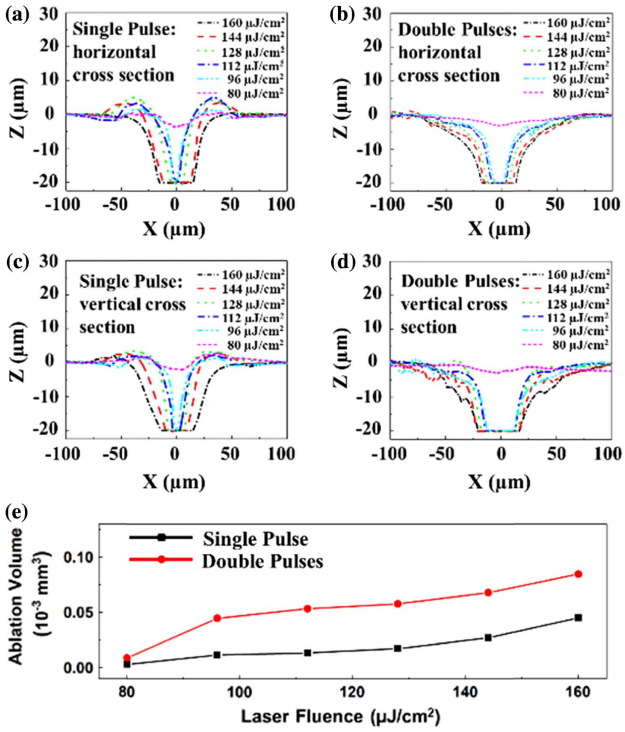

Fig. 4. (a) Horizontal and (c) vertical cross section of surface ablation on PCL film generated by single-pulse femtosecond laser irradiation at different laser fluences; (b) horizontal and (d) vertical cross section of surface ablation on PCL film generated by double-pulse femtosecond laser irradiation at 264-fs time delay and different laser fluences. (e) Ablation volume as a function of laser fluence for single and double pulses.

to the laser spot's energy distribution. For the single-pulse ablation, as shown in Figs. 4(a) and 4(c), there is an obvious hump on the edge due to heat effect-induced resolidification. However, Figs. 4(b) and 4(d) show that the edges in the ablation area are flat by using double-pulse ablation, which indicates the double-pulse-induced surface ablation is stronger compared to the single-pulse ablation.

The variation of ablation volume versus laser fluence for a single-pulse regime is shown in Fig. 4(e). In this case, the depth of the hump should be neglected. Thus, the depth is estimated as the distance from the baseline $y = 0$ to the bottom of the hole. It can be observed that the ablation volume increases from 0.32×10^{-5} to 4.5×10^{-5} mm^3, since laser fluence changes from 80 to 160 μJ/cm^2. For the double-pulses ablation, at a time delay of 264 fs, it can be found that most of the ablated craters have larger diameters with respect to the single-pulse crater, as shown in Figs. 3(g)–3(l). The corresponding heat-affected zones also become bigger. The volumes of the double-pulse laser ablation with total laser fluence from 80 to 160 μJ/cm^2 are 0.89×10^{-5}, 4.46×10^{-5}, 5.32×10^{-5}, 6.43×10^{-5}, 7.17×10^{-5}, and 8.46×10^{-5} mm^3, respectively, which are much larger than those for the single-pulse ablation, as shown in Fig. 4(e). For the irradiation of 160 μJ/cm^2 total laser fluence, the laser fluence of each subpulse is higher than the ablation threshold (80 μJ/cm^2). In this case, the SP arrives at the polymer after the FP ablation. The absorption of the SP laser energy by the polymer is enhanced due to the FP laser-induced surface modification, which results in a maximum enhancement of ablation efficiency of about $(9.06 - 4.5)/4.5 \times 100\% = 101\%$ (for detailed ablation results, see Appendix A). However, for the FP laser fluence lower than the ablation threshold at 80 μJ/cm^2, for instance, the ablation volume induced by 112 μJ/cm^2 total laser fluence (56 μJ/cm^2 for each subpulse) irradiation of the polymer can reach about 5.91×10^{-5} mm^3 at a time delay of 132 fs (for detailed ablation results, see Appendix A), which is 4.38 times the 112 μJ/cm^2 single-pulse-induced ablation (1.35×10^{-5} mm^3). Thus, the corresponding maximum increase of ablation efficiency can reach about $(5.91 - 1.35)/1.35 \times 100\% = 338\%$.

Figures 5(a)–5(f) show the ablation enhancement factors by double-pulse femtosecond laser ablation at different laser fluences. All these figures are plotted with the same y-axis scale for easy comparison. The ablation enhancement factor is defined as $\sigma = \frac{V_i}{V_o}$, where V_i and V_o are the ablated volumes by double-pulse and single-pulse ablation, respectively. It can be observed that most of the ablation by double pulses can achieve obvious enhancement with respect to the single-pulse ablation. The ablation enhancement factor is mostly larger than 1 within a 300-fs time delay, which means the double-pulse-induced ablation is more effective compared to single-pulse ablation at these time delays. However, the ablation enhancement factor reduces and is lower than 1 at time delay > 330 fs. In this case, the double-pulse femtosecond laser-induced surface ablation becomes weaker than single-pulse ablation. Furthermore, the ablation enhancement factor decreases obviously when the total laser fluence is too high at a laser fluence of 160 μJ/cm^2 [Fig. 5(f)] or too low of a laser fluence of 80 μJ/cm^2 [Fig. 5(a)]. For the 160 μJ/cm^2 double-pulse laser ablation, the FP of 80 μJ/cm^2 can generate the surface ablation. Then the absorption of the SP (80 μJ/cm^2) is enhanced by the FP-induced surface modification. However, for the subpulse with insufficient laser fluence for the surface ablation

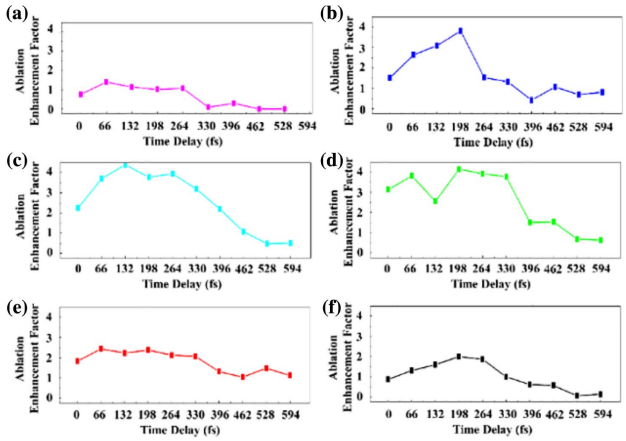

Fig. 5. Ablation enhancement factor by double-pulse laser ablation on PCL film at different laser fluences. (a) FP, 40 μJ/cm^2 and SP, 40 μJ/cm^2; (b) FP, 48 μJ/cm^2 and SP, 48 μJ/cm^2; (c) FP, 56 μJ/cm^2 and SP, 56 μJ/cm^2; (d) FP, 64 μJ/cm^2 and SP, 64 μJ/cm^2; (e) FP, 72 μJ/cm^2 and SP, 72 μJ/cm^2; (f) FP, 80 μJ/cm^2 and SP, 80 μJ/cm^2.

(lower than 80 μJ/cm^2), the FP can only melt the polymer surface. In this case, the material is required to absorb enough latent heat for the phase change from liquid to vapor. However, the absorption coefficient (α) of nonlinear optics materials is described by the equation: $\alpha \approx 2k \cdot (1 - n)$, where k is the wavenumber related to the wavelength, and n is the material's refractive index [28]. In our experiment, the wavelength is 800 nm for both the FP and the SP, which means the absorption coefficient is inversely proportional to the material's refractive index. For the PCL, the refractive index decreases with the temperature ($n = 1.463$ for 293.15 K, and $n = 1.455$ for 313.15 K) [29]. Thus, the absorption capability of melted PCL is higher than that of the solid PCL, which means the energy absorption of the SP on PCL film enhances after the FP irradiation. This enhancement of absorption can overcome the latent heat and generate considerable surface ablation. Therefore, the double-pulse laser irradiation of a total laser fluence ranging from 96 to 128 μJ/cm^2, as shown in Figs. 3(b)–3(d), can generate strong ablation enhancement compared to the case of 144 and 160 μJ/cm^2 [Figs. 5(e) and 5(f)]. However, under each subpulse of 40 μJ/cm^2 laser fluence ablation, as shown in Fig. 5(f), the enhancement of surface ablation becomes weaker. The lower laser fluence of the FP results in a weak melting effect, which leads to low absorption of the SP laser energy. In this case, the 80 μJ/cm^2 double-pulse ablation is similar to the single-pulse ablation at a time delay < 330 fs. By increasing time delay from 330 to 594 fs, the surface ablation decreases abruptly. Therefore, the surface ablation of PCL film can be well tuned by the laser fluence of the FP.

Figures 6(a)–6(c) show the single-pulse-induced surface ablation at the laser fluence from 32 to 48 μJ/cm^2. It can be observed that no very clear melting effect can be observed while the laser fluence is lower than 40 μJ/cm^2. Thus, the melting threshold is about 40 μJ/cm^2. The surface ablation can be further tuned by changing the ratio of laser fluence between the FP and the SP at the same total laser fluence. With a total laser fluence of 112 μJ/cm^2, the laser fluence of the FP is set to 32, 48, 56, 64, and 80 μJ/cm^2; meanwhile, the corresponding laser fluence of the SP is 80, 64, 56, 48, and 32 μJ/cm^2, respectively. As shown in Fig. 6(d), for an FP of 32 μJ/cm^2 and SP of 80 μJ/cm^2, the ablation enhancement can only be achieved at time delays from 0 to 66 fs, while the double-pulse ablation at time delays from 132 to 594 fs shows lower ablation volumes compared to the single pulse. In this case, the melting due to the low FP laser fluence is weaker; thus, the following pulse cannot generate considerable ablation. However, under the FP of 80 μJ/cm^2 and the SP of 32 μJ/cm^2, the ablation enhancement can be achieved at the time delay of 0–330 fs. In this condition, the 80 μJ/cm^2 FP results in surface ablation, which is beneficial to increase the absorption of the SP. Thus, 80 μJ/cm^2 FP and 32 μJ/cm^2 SP can achieve ablation enhancement within a wide range of time delay (66 to 330 fs). As shown in Fig. 6(e), the laser fluence of the FP is further changed to 48 μJ/cm^2 and 64 μJ/cm^2 at a total laser fluence of 112 μJ/cm^2. 48 and 64 μJ/cm^2 are close to the ablation threshold, and a considerable ablation enhancement can be achieved within 330 fs and then reduced with a time delay > 330 fs, which is in accordance with the results shown in Fig. 5. Therefore, temporal overlapping double-pulse irradiation can reduce the ablation threshold for the femtosecond laser ablation with a short time delay. The ablation enhancement can be well tuned by time delay and laser fluence ratio between the two subpulses.

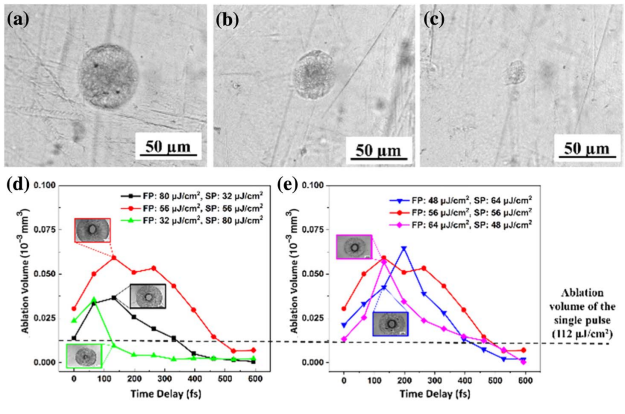

Fig. 6. Surface ablation on PCL film generated by single-pulse femtosecond laser irradiation at different laser fluences. (a) 48, (b) 40, and (c) 32 μJ/cm^2; (d), (e) ablation volumes at different laser fluence ratios for double-pulse irradiation on PCL film. The total laser fluence is kept at 112 μJ/cm^2.

4. CONCLUSION

In this paper, the surface ablation enhancement of temporal overlapping double-pulse femtosecond laser irradiation is studied at different time delays and laser fluences. The ablation enhancement mechanism is investigated by the temperature distribution model and experiment results. Compared to the single-pulse femtosecond laser ablation, the double-pulse femtosecond laser ablation can be enhanced mostly within twice the pulse duration, and then decreases with time delay. When the laser fluence of the FP is higher than the ablation threshold, the enhancement of the laser-induced surface ablation is attributed to the absorption increase induced by the FP. In the case of the subpulse laser fluence lower than the ablation threshold, the considerable ablation enhancement can also be achieved by the FP-induced absorption improvement because of the increase of avalanche ionization. The surface ablation enhancement can be further tuned by changing the ratio of two subpulse laser fluences. Under the same total laser fluence, a high laser fluence for the FP can generate more effective surface ablation. This approach provides a novel way and understanding of the efficiency increase for ultrashort laser processing.

APPENDIX A

The free-electron densities of single pulses and double pulses are calculated depending on Eqs. (1)–(3). The peak intensities of double pulses are defined as $I_1(t) = I_2(t) = I_0(t)/2$, where $I_0(t)$ is the single-pulse laser intensity. The constant $a \approx 0.01$ cm^2/(ps · GW) is the avalanche coefficient [24]. σ_k denotes the k-photon absorption cross section, and k is equal to the smallest number of photons needed to overcome the optical bandgap of the material. The energy gap of the isolator

should be larger than 4.5 eV. Thus, for the 800-nm wavelength (photon energy ~1.61 eV), the k can be defined as 3, while $\sigma^{(3)} \approx 7 \times 10^{-17}$ cm$^3 \cdot$ ps$^{-1} \cdot$ TW^{-3} [30]. Figure 7 shows the evolution of electron density induced by the single- and double-pulse irradiation for a 150-fs pulse duration and the total peak intensities from 2.5 to 10 TW/cm^2. The time delay between double pulses is set as 75 fs. For 2.5 TW/cm^2 femtosecond laser irradiation, as shown in Fig. 1(a), the single-pulse-induced free-electron density is higher compared to the double-pulse irradiation. Because multiphoton ionization is strongly intensity-dependent, the electron production takes place principally at the peak of the pulse. In this case, the FP-induced free-electron density is insufficient for the SP to quickly generate more free electrons through avalanche ionization, which means the surface ablation enhancement cannot be achieved at low laser power. Thus, the free-electron density induced by the single pulse is larger than by double pulses under low peak intensity. With increasing peak intensity from 5 to 10 TW/cm^2, as shown in Figs. 1(b)–1(d), the free-electron density induced by the FP is large enough. In this case, the avalanche ionization effect during the SP irradiation becomes stronger, and more free electrons can be generated. Although the peak intensity of each subpulse is lower than the single-pulse peak intensity, the double pulse can also induce larger electron density compared to that of the single pulse. It indicates that the double-pulse irradiation of several hundred femtoseconds' time delay is feasible to generate ablation enhancement.

Figures 8(a)–8(i) show the surface ablation generated by double-pulse femtosecond laser irradiation with time delays ranging from 0 to 594 fs. The total fluence is set as 160 μJ/cm^2, which is the same as the single-pulse ablation shown in the main text [Fig. 3(f)]. Obviously, it can be found that most of the ablated craters have larger diameters with respect to the single-pulse ablation crater. The corresponding heat-affected zones also become bigger. Since each pulse has a laser fluence of 80 μJ/cm^2, which is higher than the single-pulse ablation threshold, both pulses can achieve the polymer surface ablation. As shown in Fig. 8(j), the ablation volume

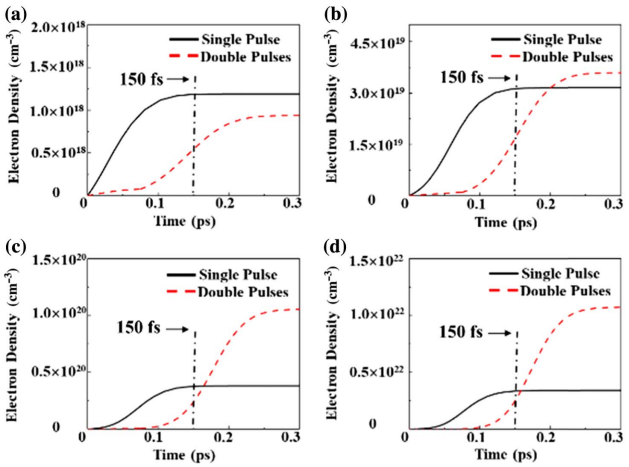

Fig. 7. Calculated evolution of free-electron density for the single pulse and double pulses (75 fs time delay) at a 150 fs, 800 nm pulse of different total peak intensities. (a) 2.5, (b) 5, (c) 7.5, and (d) 10 TW/cm^2.

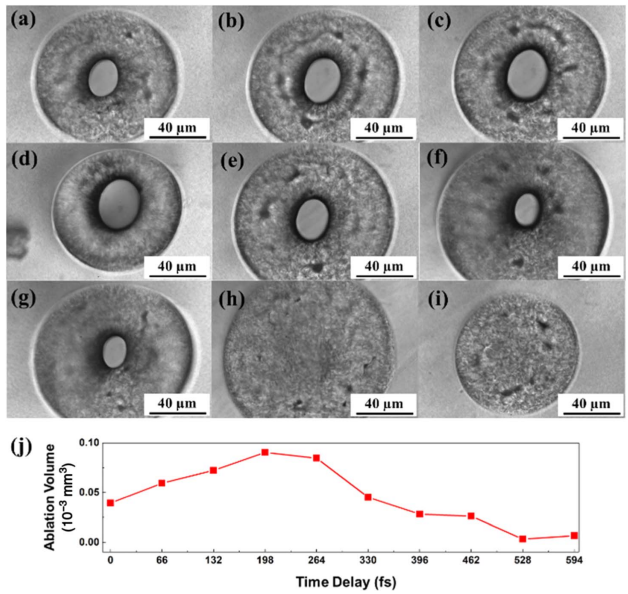

Fig. 8. Surface ablation generated by double-pulse femtosecond laser irradiation on PCL film at a total laser fluence of 160 μJ/cm^2 (FP, 80 μJ/cm^2 and SP, 80 μJ/cm^2) and different time delays of (a) 0, (b) 66, (c) 132, (d) 198, (e) 330, (f) 396, (g) 462, (h) 528, and (i) 594 fs; (j) corresponding ablation volume as a function of time delay.

first increases at a time delay of 0 to 198 fs and then decreases consistently while the time delay increases from 264 to 594 fs. At a time delay of 66, 132, 198, 264, and 330 fs, the double-pulse laser ablation volumes are 5.91×10^{-5}, 7.24×10^{-5}, 9.06×10^{-5}, 8.51×10^{-5}, and 4.52×10^{-5} mm^3, respectively, which are greater than those for the single pulse (4.5×10^{-5} mm^3). Compared with the single pulse, the double pulse consistently induces the ablation enhancement for the time delay $\tau < 330$ fs. For the time delays of $\tau = 396$, 462, 528, and 594 fs, the ablation volumes are 2.83×10^{-5}, 2.62×10^{-5}, 0.42×10^{-5}, and 0.66×10^{-5} mm^3, respectively. The ablation volume induced by the double-pulse irradiation decreases after a long time delay, which is attributed to the weakening of temporal overlapping between the FP and the SP. The above results illustrate that the time delay strongly affects the double-pulse laser ablation due to the temporal overlapping of two separate laser pulses, which is in accordance with the theoretical prediction. Compared with the laser ablation by a single laser beam at the same total laser power, the temporal overlapping double-pulse laser ablation shows enhanced ablation efficiency within a 300-fs time delay. For the 160 μJ/cm^2 total laser fluence, when there is no time delay between the double pulses, the FP and SP reach the polymer surface simultaneously. In this case, the absorption of each pulse at a laser fluence of 80 μJ/cm^2 is equal to the single pulse with the same total laser fluence. Therefore, the ablation volume of double pulses without a time delay (3.91×10^{-5} mm^3) is close to that induced by single-pulse irradiation (4.5×10^{-5} mm^3). At time delays of 60 to 330 fs, the SP arrives at the polymer after the FP ablation. The absorption of the SP by the polymer is changed due to the FP laser-induced surface modification. By increasing

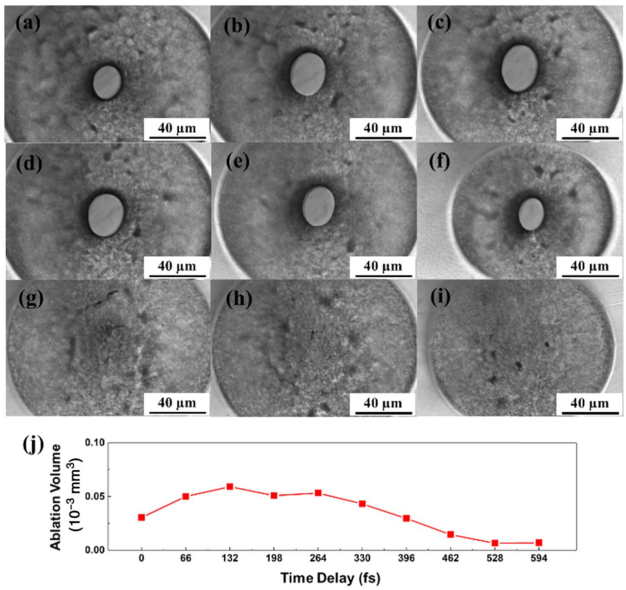

Fig. 9. Surface ablation generated by double-pulse femtosecond laser irradiation on PCL film at a total laser fluence of 112 μJ/cm^2 (FP, 56 μJ/cm^2 and SP, 56 μJ/cm^2) and different time delays of (a) 0, (b) 66, (c) 132, (d) 198, (e) 330, (f) 396, (g) 462, (h) 528, and (i) 594 fs; (j) corresponding ablation volume as a function of time delay.

the time delay to 150 fs (laser pulse duration), the temporal overlapping between the FP and SP decreases. Therefore, the enhancement of surface ablation effect reduces for a time delay > 330 fs.

The surface ablation generated by double-pulse femtosecond laser ablation at a total laser fluence of 112 μJ/cm^2 is shown in Figs. 9(a)–9(i). Similarly, the 112 μJ/cm^2 laser double-pulse-induced ablation first increases at a short time delay, from 66 to 330 fs. The average ablation volumes are 4.53×10^{-5}, 5.01×10^{-5}, 5.93×10^{-5}, 5.09×10^{-5}, 5.33×10^{-5}, 4.32×10^{-5} mm^3 at a time delay of 0, 66, 132, 198, 264, and 330 fs, respectively. Then the laser ablation reduces for the time delay > 398 fs. In this case, the average ablation volumes are 2.97×10^{-5}, 1.45×10^{-5}, 0.70×10^{-5}, and 0.66×10^{-5} mm^3, while the time delays are 396, 462, 528, and 594 fs, respectively. However, the double-pulse ablation volume (>1.45×10^{-5} mm^3) under 112 μJ/cm^2 laser fluence is higher than the single-pulse ablation (1.35×10^{-5} mm^3) at a time delay of 462 fs.

Funding. National Research Foundation Singapore (A1883c0010); National Natural Science Foundation of China (51975017); China Scholarship Council.

Acknowledgment. We wish to thank Dr. Yang Li and Dr. Huagang Liu for the discussions on double-pulse laser experiments. The support provided by China Scholarship Council (CSC) during a visit of Zhenyuan Lin to the National University of Singapore is acknowledged.

Disclosures. The authors declare no conflicts of interest.

REFERENCES

1. B. N. Chichkov, C. Momma, S. Nolte, F. von Alvensleben, and A. Tiinnermann, "Femtosecond, picosecond and nanosecond laser ablation of solids," Appl. Phys. A **63**, 109–115 (1996).
2. T. C. Chong, M. H. Hong, and L. P. Shi, "Laser precision engineering: from microfabrication to nanoprocessing," Laser Photon. Rev. **4**, 123–143 (2010).
3. K. Sokolowski-Tinten, J. Bialkowski, A. Cavalleri, D. von der Linde, A. Oparin, J. Meyer-ter-Vehn, and S. I. Anisimov, "Transient states of matter during short pulse laser ablation," Phys. Rev. Lett. **81**, 224–227 (1998).
4. P. Lorazo, L. J. Lewis, and M. Meunier, "Short-pulse laser ablation of solids: from phase explosion to fragmentation," Phys. Rev. Lett. **91**, 225502 (2003).
5. M. E. Povarnitsyn, K. V. Khishchenko, and P. R. Levashov, "Phase transitions in femtosecond laser ablation," Appl. Surf. Sci. **255**, 5120–5124 (2009).
6. D. Perez and L. J. Lewis, "Ablation of solids under femtosecond laser pulses," Phys. Rev. Lett. **89**, 255504 (2002).
7. R. Zhou, S. D. Lin, Y. Ding, H. Yang, K. O. Y. Keng, and M. H. Hong, "Enhancement of laser ablation via interacting spatial double-pulse effect," Opto-Electron. Adv. **1**, 18001401 (2018).
8. F. Fraggelakis, G. Mincuzzi, J. Lopez, I. Manek-Hönninger, and R. Kling, "Controlling 2D laser nano structuring over large area with double femtosecond pulses," Appl. Surf. Sci. **470**, 677–686 (2019).
9. S. A. Jalil, J. Yang, M. ElKabbash, S. C. Singh, and C. Guo, "Maskless formation of uniform subwavelength periodic surface structures by double temporally-delayed femtosecond laser beams," Appl. Surf. Sci. **471**, 516–520 (2019).
10. Y. Ding, L. J. Yang, and M. H. Hong, "Enhancement of pulsed laser ablation assisted with continuous wave laser irradiation," Sci. China Phys. Mech. Astron. **62**, 034211 (2019).
11. F. Banhart, J. Kotakoski, and A. V. Krasheninnikov, "Structural defects in graphene," ACS Nano **5**, 26–41 (2011).
12. A. C. Forsman, P. S. Banks, M. D. Perry, E. M. Campbell, A. L. Dodell, and M. S. Armas, "Double-pulse machining as a technique for the enhancement of material removal rates in laser machining of metals," J. Appl. Phys. **98**, 033302 (2005).
13. T. Donnelly, J. G. Lunney, S. Amoruso, R. Bruzzese, X. Wang, and X. Ni, "Double pulse ultrafast laser ablation of nickel in vacuum," J. Appl. Phys. **106**, 013304 (2009).
14. Y. Qi, H. Qi, Q. Wang, Z. Chen, and Z. Hu, "The influence of double pulse delay and ambient pressure on femtosecond laser ablation of silicon," Opt. Laser Technol. **66**, 68–77 (2015).
15. M. Qiao, J. Yan, and B. Gao, "Ablation of TiO_2 surface with a double-pulse femtosecond laser," Opt. Commun. **441**, 49–54 (2019).
16. T. Y. Choi, D. J. Hwang, and C. P. Grigoropoulos, "Femtosecond laser induced ablation of crystalline silicon upon double beam irradiation," Appl. Surf. Sci. **197–198**, 720–725 (2002).
17. M. D. Perry, B. C. Stuart, P. S. Banks, M. D. Feit, V. Yanovsky, and A. M. Rubenchik, "Femtosecond laser induced ablation of crystalline silicon upon double beam irradiation," J. Appl. Phys. A **85**, 6803–6810 (1999).
18. J. Krüger and W. Kautek, "Ultrashort pulse laser interaction with dielectrics and polymers," in *Polymers and Light*, Vol. **168** of Advances in Polymer Science (Springer, 2004), pp. 247–290.
19. M. Lenzner, J. Krüger, S. Sartania, Z. Cheng, C. Spielmann, G. Mourou, W. Kautek, and F. Krausz, "Femtosecond optical breakdown in dielectrics," Phys. Rev. Lett. **80**, 4076–4079 (1998).
20. T. Nagata, M. Kamata, and M. Obara, "Optical waveguide fabrication with double pulse femtosecond lasers," Appl. Phys. Lett. **86**, 251103 (2005).
21. I. H. Chowdhury, X. Xu, and A. M. Weiner, "Ultrafast double-pulse ablation of fused silica," Appl. Phys. Lett. **86**, 151110 (2005).
22. A. Semerok and C. Dutouquet, "Ultrashort double pulse laser ablation of metals," Thin Solid Films **453–454**, 501–505 (2004).
23. E. I. Ageev, V. Y. Bychenkov, A. A. Ionin, S. I. Kudryashov, A. A. Petrov, A. A. Samokhvalov, and V. P. Veiko, "Double-pulse femtosecond laser peening of aluminum alloy AA5038: effect of inter-pulse

delay on transient optical plume emission and final surface microhardness," Appl. Phys. Lett. **109**, 211902 (2016).
24. B. C. Stuart, M. D. Feit, A. M. Rubenchik, B. W. Shore, and M. D. Perry, "Laser-induced damage in dielectrics with nanosecond to subpicosecond pulses," Phys. Rev. Lett. **74**, 2248–2251 (1995).
25. T. K. Dash and V. B. Konkimalla, "Poly-epsilon-caprolactone based formulations for drug delivery and tissue engineering: a review," J. Control. Release **158**, 15–33 (2012).
26. K. Xu, Z. Wang, C. F. Tan, N. Kang, L. Chen, L. Ren, E. S. Thian, G. W. Ho, R. Ji, and M. Hong, "Uniaxially stretched flexible surface plasmon resonance film for versatile surface enhanced Raman scattering diagnostics," ACS Appl. Mater. Interfaces **9**, 26341–26349 (2017).
27. K. S. Tiaw, S. W. Goh, M. Hong, Z. Wang, B. Lan, and S. H. Teoh, "Laser surface modification of poly(epsilon-caprolactone) (PCL) membrane for tissue engineering applications," Biomaterials **26**, 763–769 (2005).
28. W. Knoll, "Optical properties of polymers," in *Materials Science and Technology* (VCH, 1993), pp. 529–594.
29. U. M. Fornefeld-Schwarz and P. Svejda, "Refractive indices and relative permittivities of liquid mixtures of gamma-butyrolactone, gamma-valerolactone, delta-valerolactone, or epsilon-caprolactone plus benzene, plus toluene, or plus ethylbenzene at 293.15 K and 313.15 K and atmospheric pressure," J. Chem. Eng. Data **44**, 597–604 (1999).
30. S. C. Jones, P. Braunlich, R. T. Casper, and X. A. Shen, "Recent progress on laser-induced modifications and intrinsic bulk damage of wide-gap optical materials," Opt. Eng. **28**, 281039 (1989).